JACS
JOURNAL OF THE AMERICAN CHEMICAL SOCIETY

Article

Palladium-catalyzed *meta*-C–H allylation of arenes: A unique combination of pyrimidine-based template and hexafluoroisopropanol

Sukdev Bag, Surya K, Arup Mondal, Ramasamy Jayarajan, Uttam Dutta, Sandip Porey, Raghavan B. Sunoj, and Debabrata Maiti

J. Am. Chem. Soc., **Just Accepted Manuscript** • DOI: 10.1021/jacs.0c05223 • Publication Date (Web): 04 Jun 2020

Just Accepted

is published by the American Chemical Society. 1155 Sixteenth Street N.W., Washington, DC 20036

Palladium-catalyzed *meta*-C–H allylation of arenes: A unique combination of pyrimidine-based template and hexafluoroisopropanol

Sukdev Bag, Surya K, Arup Mondal, Ramasamy Jayarajan, Uttam Dutta, Sandip Porey, Raghavan B. Sunoj,* and Debabrata Maiti*

Department of Chemistry, Indian Institute of Technology Bombay, Powai, Mumbai 400076, India

ABSTRACT: Controlling remote selectivity and delivering novel functionalities at distal positions in arenes are an important endeavor in contemporary organic synthesis. In this vein, template engineering and mechanistic understanding of new functionalization strategies are essential for enhancing the scope of such methods. Herein, *meta*-C–H allylation of arenes has been achieved with the aid of palladium catalyst, pyrimidine-based auxiliary and allyl phosphate. 1,1,1,3,3,3-Hexafluoroisopropanol (HFIP) was found as a critical solvent in this transformation. The role of HFIP throughout catalytic cycle has been systematically studied. A broad substrate scope with phenethyl ether, phenol, benzylsulfonyl ester, phenethylsulfonyl ester, phenylacetic acid, hydrocinnamic acid and 2-phenylbenzoic acid derivatives have been demonstrated. Interestingly, conformationally flexible arenes have also been selectively allylated at *meta*-position using allyl phosphate. A combination of ^{1}H NMR, ^{31}P NMR, ESI-MS, kinetic experiments, and density functional theory (DFT) computations suggested that reaction proceeds through a ligand-assisted *meta*-C–H activation, allyl addition forming a Pd-π-allyl complex which is then followed by a turn-over determining C–C bond formation step leading to the *meta*-allylated product.

INTRODUCTION

Allylation can be considered as one of the most important organic transformations owing to the prevalence of the allyl group in drug molecules and their ease of transformation to other functional groups.[1] Various methods for allylation have been formulated to address the ever-increasing demands from the synthetic communities (Figure 1a). A classic example of *ortho*-allylation is Claisen rearrangement of allylphenol ether.[2] In the case of *ortho*-substituted allyl phenol ethers, one can obtain *para*-allylic phenol derivatives through Cope rearrangement.[2c,3] Alternatively, the more straight forward Friedel–Crafts allylation has been achieved using Lewis acids.[4] However, these methods are limited to electronically-biased arenes, and often produce a mixture of regioisomers and/or over-allylated products. In this regard, Tsuji-Trost allylation has been considered as the most versatile allylation reaction where nucleophilic coupling partners have been utilized considering soft/hard nature.[5] To address the selectivity issues, an array of practical directing groups (DGs) has been developed to achieve proximal *ortho*-C–H allylation of arenes using transition metal catalysts.[6] However, terminal *meta*-C–H allylation of arenes has not been realized, despite an adequate number of reports on directed and non-directed allylation.

While an innate functional group and/or an installed DG allows transition metal to access the immediate aryl C–H bond,[7] distal C–H bonds that are geometrically farther from the DG are challenging to functionalize in a selective manner making them rather inaccessible.[8] In this endeavor, nitrile-based template has been modulated to achieve the first *meta*-selective functionalization by Yu and coworkers.[9] Our group has reported the *para*-C–H functionalization of arenes.[10] Distance and geometry play major roles in remote selectivity. Additionally, if there is regio-

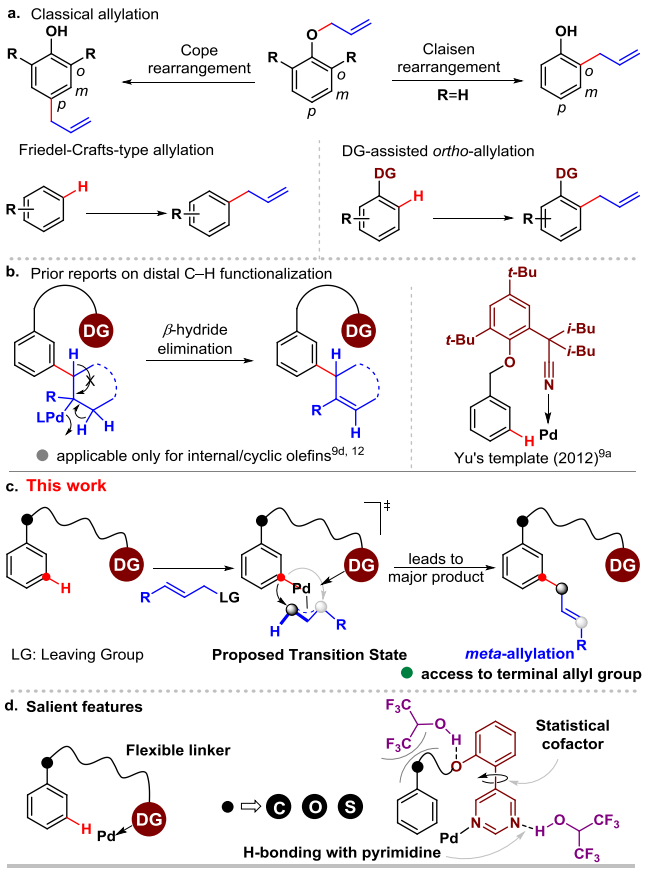

Figure 1. (a) Classical allylation reactions. (b) Prior reports. (c) The present work; Formation of major allylated product by proposed transition state. (d) Pyrimidine DG.

switchable coupling partner, it adds further to the difficulties with the existing issues.[11] Taking cognizance of the increasing demands for the design of newer templates and tunable DGs, we became interested in developing a valuable *meta*-allyation protocol for various arenes (Figure 1b and 1c).[12] In our previous report[9d] on olefination with activated olefins, we have observed allylation product formation with cyclic activated olefins. With cyclic olefins, 1,2-migratory insertion of palladium followed by *β*-hydride elimination from less hindered secondary carbon center delivers the allylation products. Such a reaction is mechanistically distinct compare to the present study and it is only applicable for cyclic olefins. Most importantly, linear acyclic allylation product formation is not feasible.

RESULTS AND DISCUSSION

Reaction and template optimization. Although the nitrile-based template has shown a new direction in distal C–H functionalization, reactions are limited due to weak coordinating ability of nitrile group. Subsequently, we aimed to explore heterocycle-containing DGs which can hold metal strongly and would deliver the desired functionality selectively at *meta*- position. Notably, our recently developed pyrimidine-based DG was found to be the most effective so far for a variety of functionalizations at *meta*- position.[9f] Therefore, our investigations for the desired *meta*-allylation started with pyrimidine-based scaffold **1** and allyl alcohol in the presence of Lewis acids (Table 1). Unfortunately, initial attempts did not deliver any allylation product. Subsequently, we have varied different allylating reagents such as allyl chloride/bromide, carbonate, pivalate, etc.[13] Detailed studies revealed a trace amount of allylation product by using allyl acetate and tosylate. Subsequently, allyl phosphate has yielded promising *meta*-allylation in the presence of palladium(II) acetate and mono-protected amino acid (MPAA) ligand. Upon studying several MPAAs, *N*-Ac-Gly-OH and *N*-Form-Gly-OH were found to be the effective ligands (Table 1, entries 1 and 2); out of these two, *N*-Ac-Gly-OH proved to be superior (see Supporting Information). As solvent plays a very important role in distal C–H functionalization, we then focused on solvent optimization. Polar protic solvents such as 1,1,1,3,3,3-hexafluoroisopropanol (HFIP) and 2,2,2-trifluoroethanol (TFE) showed effectiveness towards *meta*-C–H allylation whereas 1,2-dichloroethane (DCE) slowed down the reaction. The combination of DCE and HFIP enhanced the reactivity as well as selectivity (entry 5). The high solubility of polar aprotic solvent DCE might be influencing the product formation (entry 4). No desired product was detected when tetrahydrofuran (THF) was used as a solvent (entry 6). The coordinating ability of acetonitrile with palladium might be the reason for a noticeable product formation albeit less yield compared to HFIP (entry 7). From all of these results we anticipated that HFIP is playing a critical role as hydrogen-bonding (H-bonding) donor. This polar solvent is likely to have another role as well such as stabilization of the ionic intermediates. In this article, we have systematically studied the importance of HFIP throughout the catalytic cycle (*vide infra*). Use of silver(I) acetate (AgOAc) instead of silver(I) carbonate (Ag_2CO_3) improved the yield remarkably. We assumed that either acetate-bridge between palladium-and-silver or exchangeable counter anions (*i.e.*, acetate ion from AgOAc and phosphate ion from allyl phosphate) is responsible for this observation (*vide infra*). A slight improvement in the yield was observed when sodium triflate was included as an additive. Increase of the allyl phosphate amount, reaction time along with lowering the temperature to 90 °C led to the best optimized yield for **7a** (71%; *m*:others, 15:1). The desired allylation product was isolated with 68% yield as the non-separable mixture of *meta*:others ratio of 15:1 and 21% of starting material was recovered.

Table 1. Discovering effective allylating reagent, optimization of reaction conditions and study with different DG[13]

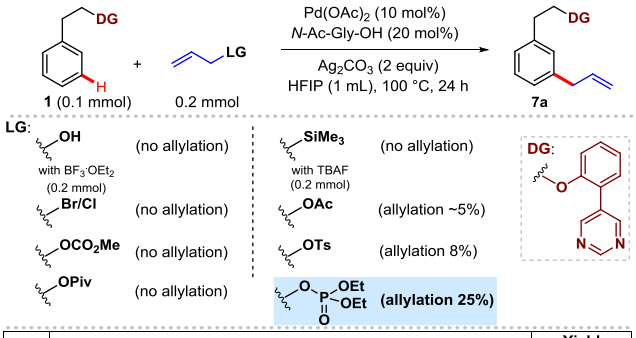

Entry	Reaction conditions	Yield (*m*:others)
1[a]	Ag_2CO_3 (2 equiv), HFIP, 100 °C, 24 h	25% (15:1)
2	*N*-Form-Gly-OH (20 mol%) instead of *N*-Ac-Gly-OH in entry 1	21% (15:1)
3	TFE instead of HFIP in entry 1	17% (15:1)
4	DCE instead of HFIP in entry 1	12% (13:1)
5	DCE+HFIP (1:1) instead of HFIP in entry 1	18% (15:1)
6	THF instead of HFIP in entry 1	nd
7	MeCN instead of HFIP in entry 1	16% (10:1)
8	AgOAc (3 equiv) instead of Ag_2CO_3 in entry 1	47% (15:1)
9	NaOTf (1 equiv) in entry 8	52% (15:1)
10[b]	90 °C instead of 100 °C in entry 9	66% (15:1)
11	30 h instead of 24 h in entry 10	71% (15:1)

Optimized reaction condition:

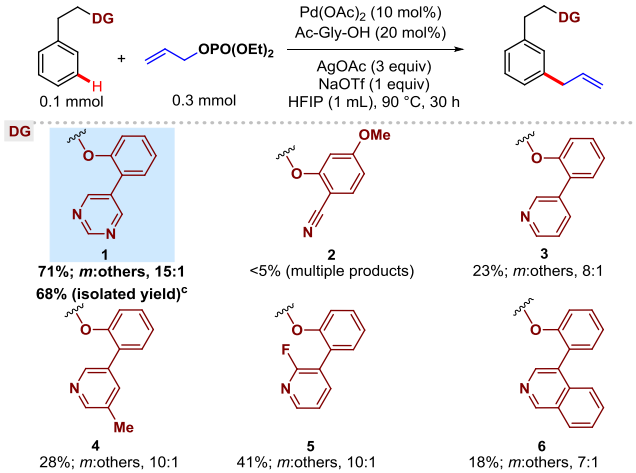

[a]$Pd(OAc)_2$ (10 mol%), Ac-Gly-OH (20 mol%), allyl phosphate (0.2 mmol); [b]allyl phosphate (0.3 mmol); [c]Yield is combined yield of isomeric mixtures of **7a**. LG, Leaving Group; *N*-Form-Gly-OH, *N*-formyl glycene.

Next, we systematically tested various templates to improve the yield and *meta*-selectivity. The nitrile-based scaffold **2** has failed to deliver the desired allylation product (Table 1). The prospect of weak coordination and unpredictable binding mode of nitrile has led us to further explore various substitutions on

Scheme 1. Scope with phenethyl alcohol derivatives[13]

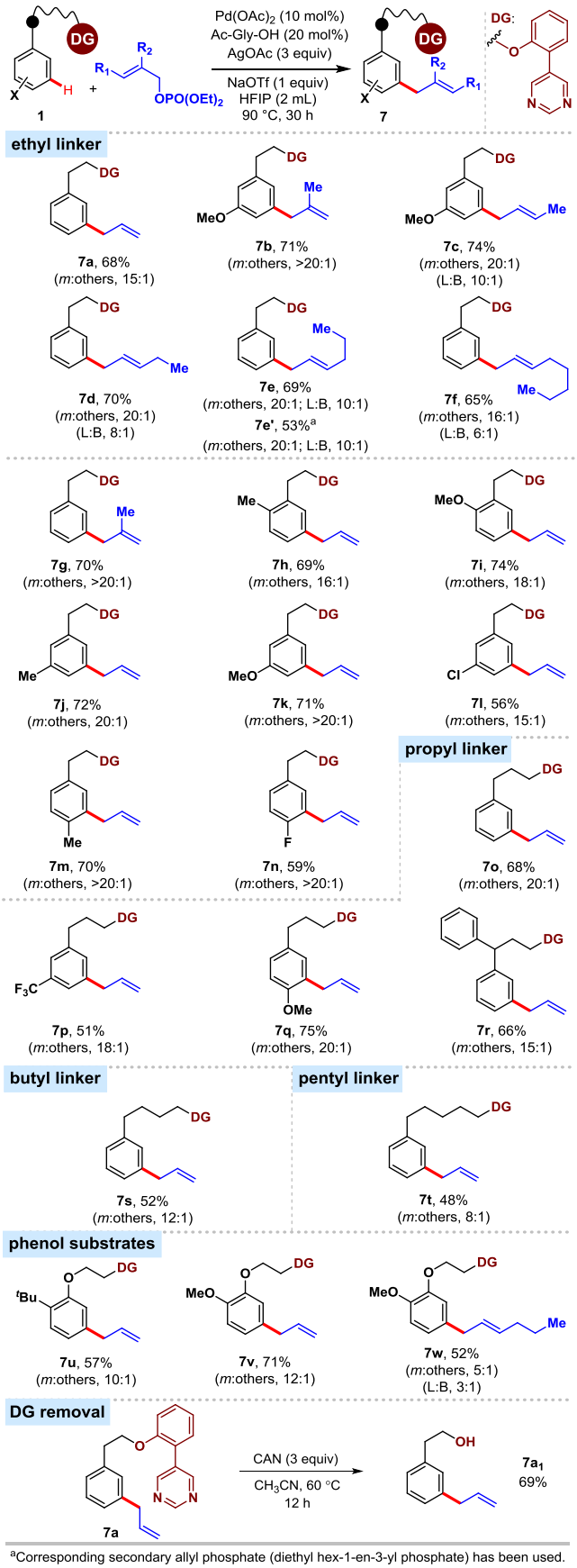

[a]Corresponding secondary allyl phosphate (diethyl hex-1-en-3-yl phosphate) has been used.

the heterocycles.[9f,14] The unsubstituted pyridine **3** and isoquinoline-based **6** delivered the allylation product in moderate yields. Electron-poor fluorine-substitution over pyridine moiety **5** afforded better yield as compared to the electron-rich methyl-substituted pyridine **4**. However, pyrimidine-based **1** was found to be the most suitable choice.[9f,15]

Scope of *meta*-C–H allylation. Having learned the optimized reaction conditions using pyrimidine-based template, we explored the scope of allylation with differently substituted allyl coupling partners (Scheme 1). Simple allyl and *β*-methyl allyl phosphate have produced exclusive *meta*-allylation in 68% (**7a**) and 71% (**7b**) isolated yields, respectively. The *γ*- methyl (**7c**), *γ*-ethyl (**7d**), *γ*-propyl (**7e**) and *γ*-pentyl (**7f**) substituted allyl phosphates provided good yield and excellent *meta*-selective allylation with promising linear/branched ratios. In case of entries 7e and 7e', we used terminal (primary) allyl phosphate and internal (secondary) allyl phosphate, respectively. But we observed the linear allylation as the major product (L:B, 10:1 for both cases). These observations suggest: (1) The product was formed through a common reversible η^1-η^3 isomerized allyl-Pd(π)-complex and (2) the linear:branched ratio was most likely governed by steric hindrance between appended *n*-propyl chain in allyl moiety and palladium coordination sphere.[13]

Subsequently, various aryl coupling partners have been evaluated under the optimized reaction conditions (Scheme 1). *Ortho*-substituted electron-rich arenes (**7h** and **7i**) preferentially delivered allylation at sterically less hindered *meta*-position with good yield and excellent selectivity. Interestingly, exclusive *meta*-allylation product has been obtained for **7j** and **7k**. Moreover, sterically encumbered *para*-substituted arenes also provided selective *meta*-allylation product (**7m**) with synthetically useful yield. We decided to fine-tune the linker length between the DG and the target arene. To validate the efficacy of pyrimidine-based DG, the chain-length has been gradually elongated from two to three, four and five-methylene-bridge with appended arene substrate. Intriguingly, good yield and high *meta*-selectivity have been observed even with five-carbon ether-linked substrates (**7o**-**7t**). Phenols are electronically-biased for *ortho*- and *para*-directed functionalization. To overcome this limitation, the template-backbone has been tuned with two ether linkages appended to the pyrimidine DG. *Ortho*-*tert*-butyl-substituted phenol (**7u**) provided 57% yield with major *meta*-selective allylation products. The current protocol can be expanded to include versatile starting precursors for the synthesis of natural products such as eugenol derivative (**7v**) with preparative yield and promising *meta*-selectivity. Although we have observed a satisfactory result with chloro-substituted aryl scaffold (**7l**), *meta*-bromo-substituted phenethyl ether provided a much lower yield (<10%) whereas iodo-substituted arene did not provide the desired product. Such reactivity can be explained as palladium might react with aryl halides such as ArBr, ArI, etc. The ether linkage of product **7a** was cleaved using ceric ammonium nitrate (CAN) to obtain *meta*-allylated phenethyl alcohol (**7a$_1$**).[16]

Sulfonyl-ester-linked benzyl (**9a**-**9c**), phenethyl (**9d**-**9h**) and phenpropyl substrate (**9i**) have been examined with allyl and substituted allyl coupling partners, which also provided *meta*-selective allylation products with promising yield (Scheme 2). Various natural products and drug molecules contain phenylacetic acid core structure. Substituted phenylacetic acids have

Scheme 2. Scope with sulfonyl and carbonyl ester-based scaffolds and removal of DG[13]

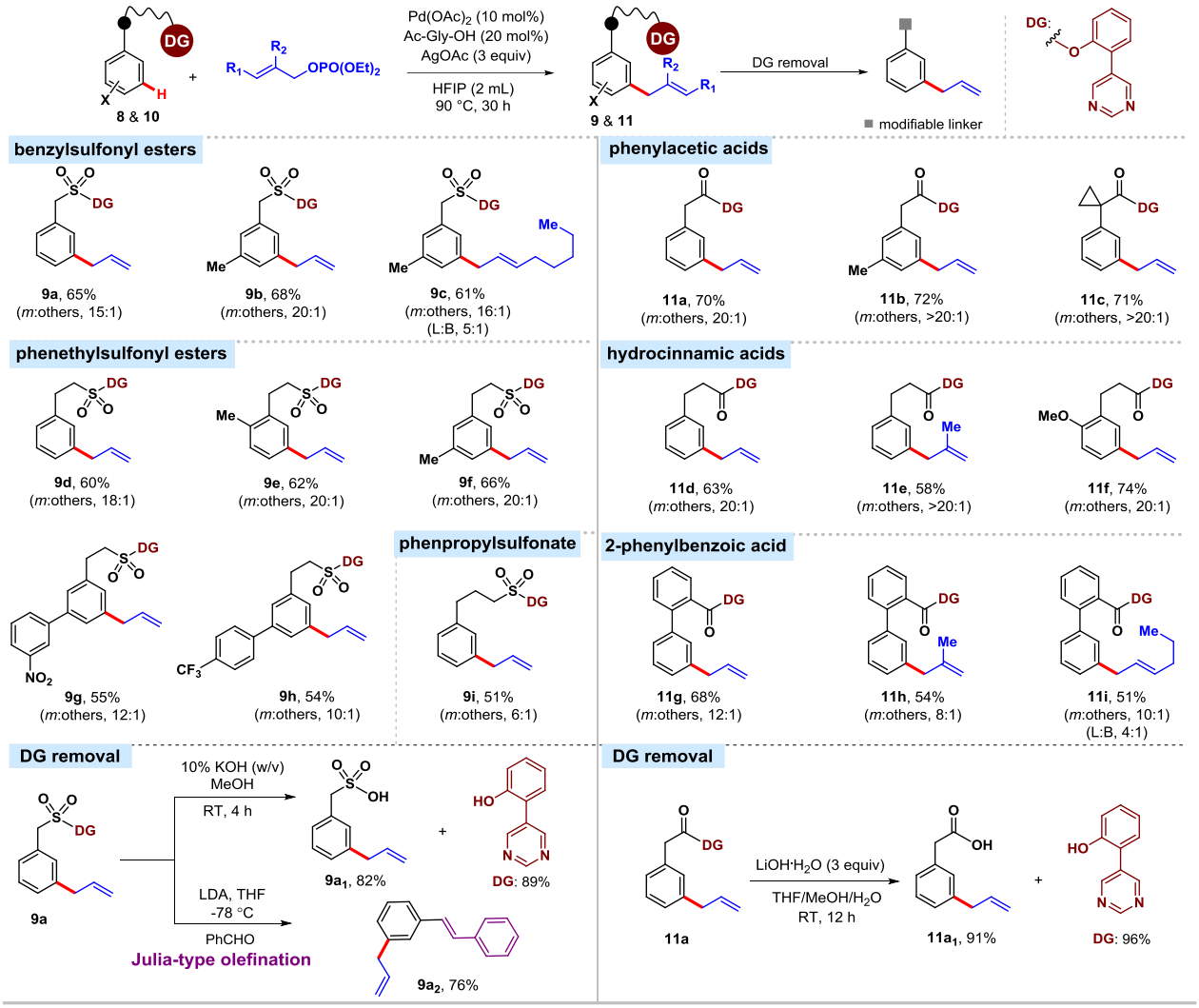

been evaluated under the optimized conditions and provided selective *meta*-allylation products (**11a-11c**). For ester scaffolds, we excluded the additive because of slight deviation of the expected yield which is due to DG cleavage. Furthermore, hydrocinnamic acid derivatives (**11d-11f**) also provided *meta*-allylation product in good yield and excellent selectivity (Scheme 2). Distal selective C–H bond functionalization of complex molecular structure is one of the important goals in this approach. 2-Phenyl benzoic acid substrate has been taken to fulfill the practicability of pyrimidine-based template and the standard reaction provided moderate to good yield and excellent selectivity with differently substituted allyl coupling partners (**11g-11i**). Removal of the DG was demonstrated using basic hydrolysis conditions with selected examples of products. *Meta*-allylation products of phenylmethanesulfonic acid (**9a$_1$**) and phenylacetic acid (**11a$_1$**) were obtained in synthetically useful yield (82% and 91%, respectively) under different basic conditions (Scheme 2). Versatility of the sulfonyl ester moiety has been further presented by converting to styrenyl product (**9a$_2$**) *via* Julia-type olefination.

Mechanistic studies. Based on our experimental observations, we hypothesize that solvent HFIP might exert a relatively more critical role in the C–H bond activation step as compared to the other steps in the case of pyrimidine-DG.[17, 18] To validate this, systematic ^{1}H NMR experiments were carried out as summarized in Figure 2. Successive introduction of the catalyst, HFIP, and mono-protected amino acid ligand *N*-Ac-Gly-OH was performed to the substrate dissolved in $CDCl_3$ and the spectrum was recorded after each such addition. We have observed a change in the overall splitting pattern of the substrate 3-methyl phenethyl ether after the addition of palladium(II) acetate (Figure 2b).[13] This observation suggests the formation of a substrate-palladium coordination complex. However, we could not observe any pronounced splitting pattern for C–H activation in the target aromatic region (highlighted in blue-dotted box). In the above-mentioned mixture, we added silver(I) acetate (Figure 2c) to detect possible palladium-silver bimetallic cluster mediated C–H activation intermediate.[9b] Although clear assignment of *meta*-carbopalladated intermediate was not feasible, the overall changes in NMR spectra and the rise of three singlet patterns along with other multiplets indicate the involvement of silver salt in the C–H activation to some extent. These observations suggest that silver acetate is likely to be involved in the carbopalladation step of the reaction. Interestingly, in the

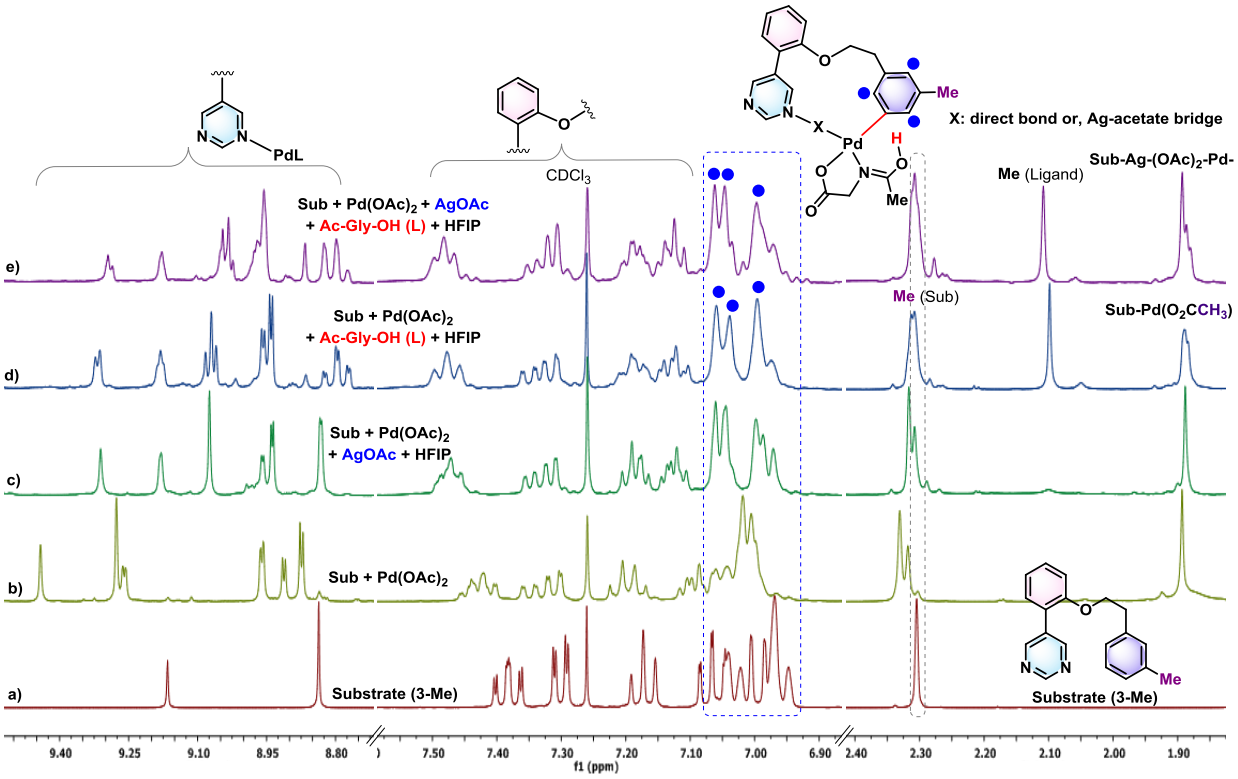

Figure 2. *Meta*-C–H bond activation followed by carbopalladation. (a) ^{1}H NMR of substrate, (b) mixture of substrate and palladium acetate, (c) mixture of substrate, palladium acetate and silver acetate, (d) after addition of *N*-Ac-Gly-OH and HFIP in the mixture of substrate and palladium acetate, (e) after addition of *N*-Ac-Gly-OH and HFIP in c.

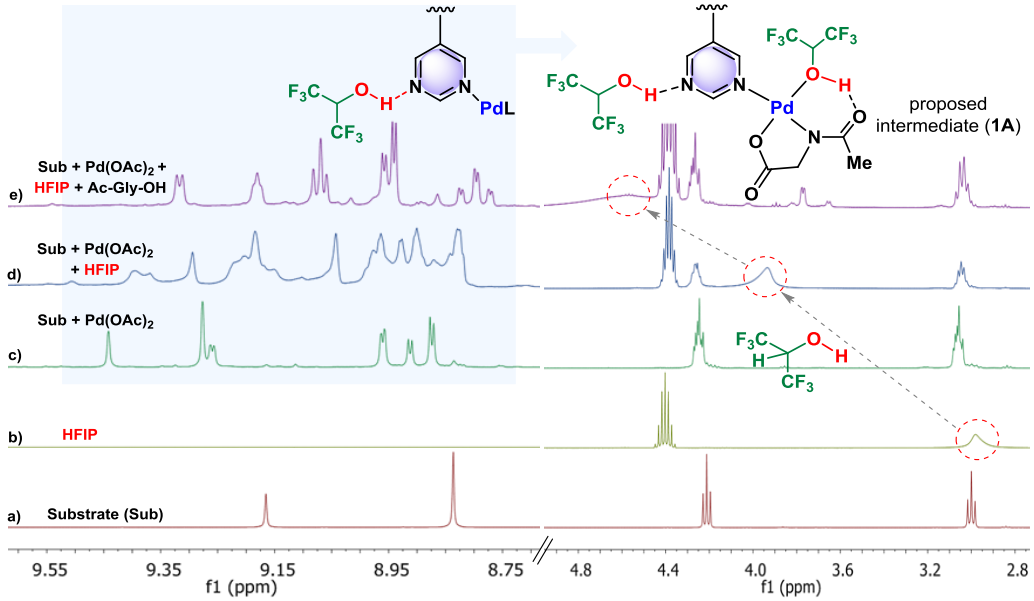

Figure 3. H-bonding with substrate-palladium intermediate. (a) ^{1}H NMR of substrate, (b) HFIP, (c) mixture of substrate and palladium acetate, (d) after addition of HFIP in the mixture of substrate and palladium acetate, (e) after addition of *N*-Ac-Gly-OH and HFIP in the mixture of substrate and palladium acetate.

presence of *N*-Ac-Gly-OH and HFIP, three clear singlets are visible in the target aromatic region (Figure 2d) that suggests the formation of carbopalladation intermediate which might have followed a concerted-metallation deprotonation (CMD) mechanism to abstract proton.[19] Furthermore, we have performed ^{1}H NMR study in the presence of palladium(II) acetate, silver(I) acetate and *N*-Ac-Gly-OH (Figure 2e). Although there is an indication of three singlets, AgOAc is likely playing less crucial role in the C–H activation step as $Pd(OAc)_2$ and *N*-Ac-Gly-OH can do the same job.

The role of HFIP all through the catalytic cycle appears to be substantial. Detail analysis suggests the presence of H-bonding interactions at the DG site as well as with the metal center and

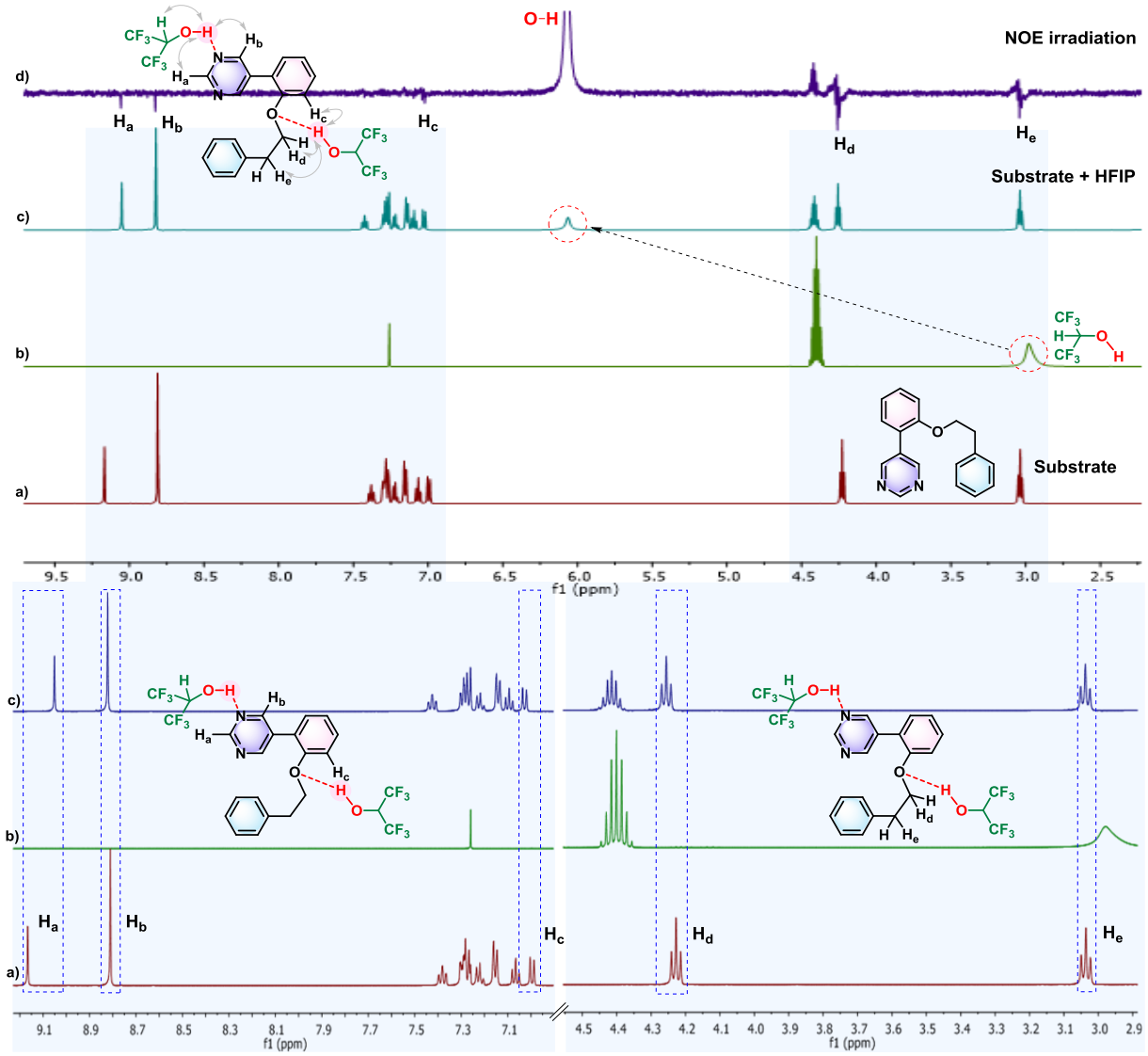

Figure 4. H-bonding between substrate and HFIP. (a) ^{1}H NMR of substrate, (b) HFIP, (c) after addition of HFIP into the solution of substrate in $CDCl_3$, (d) 1D NOE of c.

ligand (Figure 3).[13,17 and 18] Change in ^{1}H NMR pattern in the pyrimidine region (blue shaded box) and shifting of the OH peak of HFIP are strong indications of this aspect. Due to the extra electron-withdrawing nitrogen atom, pyrimidine can act as a σ-donor as well as a better *π*-acceptor ligand that might assist the coordination between palladium and oxygen atom of HFIP. Our DFT studies suggested that binding of the substrate to Pd through one of the pyrimidine nitrogen atoms is energetically more preferred for the formation of catalyst-substrate complex **1A** (shown in Figure 11). Certain interesting features of the ether-linked pyrimidine-based DG are worth noting at this juncture. The pyridyl nitrogen as well as the ether oxygen can engage in hydrogen bonding with the solvent HFIP. Consequently, bulky HFIP might play a key role to allow the target *meta*-position conformationally more populated towards directing moiety. In this context, H-bonding of HFIP with phenethyl ether scaffold has been demonstrated by ^{1}H NMR and 1D NOE correlation spectra (Figure 4). Upon irradiation, -OH peak of HFIP showed a clear interaction with neighboring protons (Figure 4d). The bottom stacked spectra are zoom-in region of the

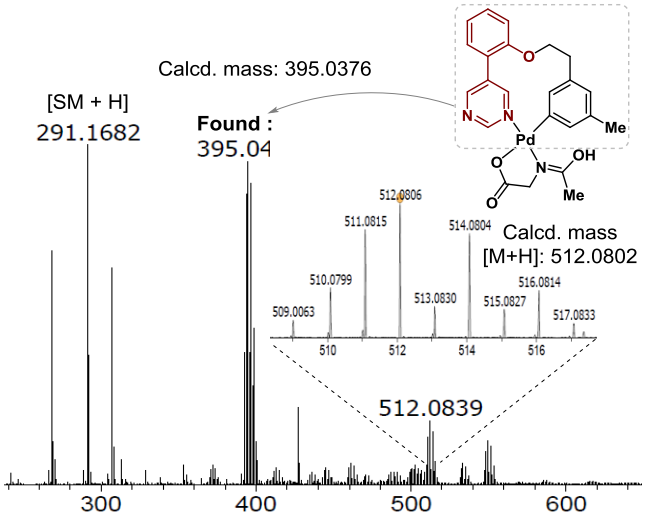

Figure 5. ESI-MS of *meta*-carbopalladated macrocyclic intermediate with *N*-Ac-Gly-OH ligand binding.

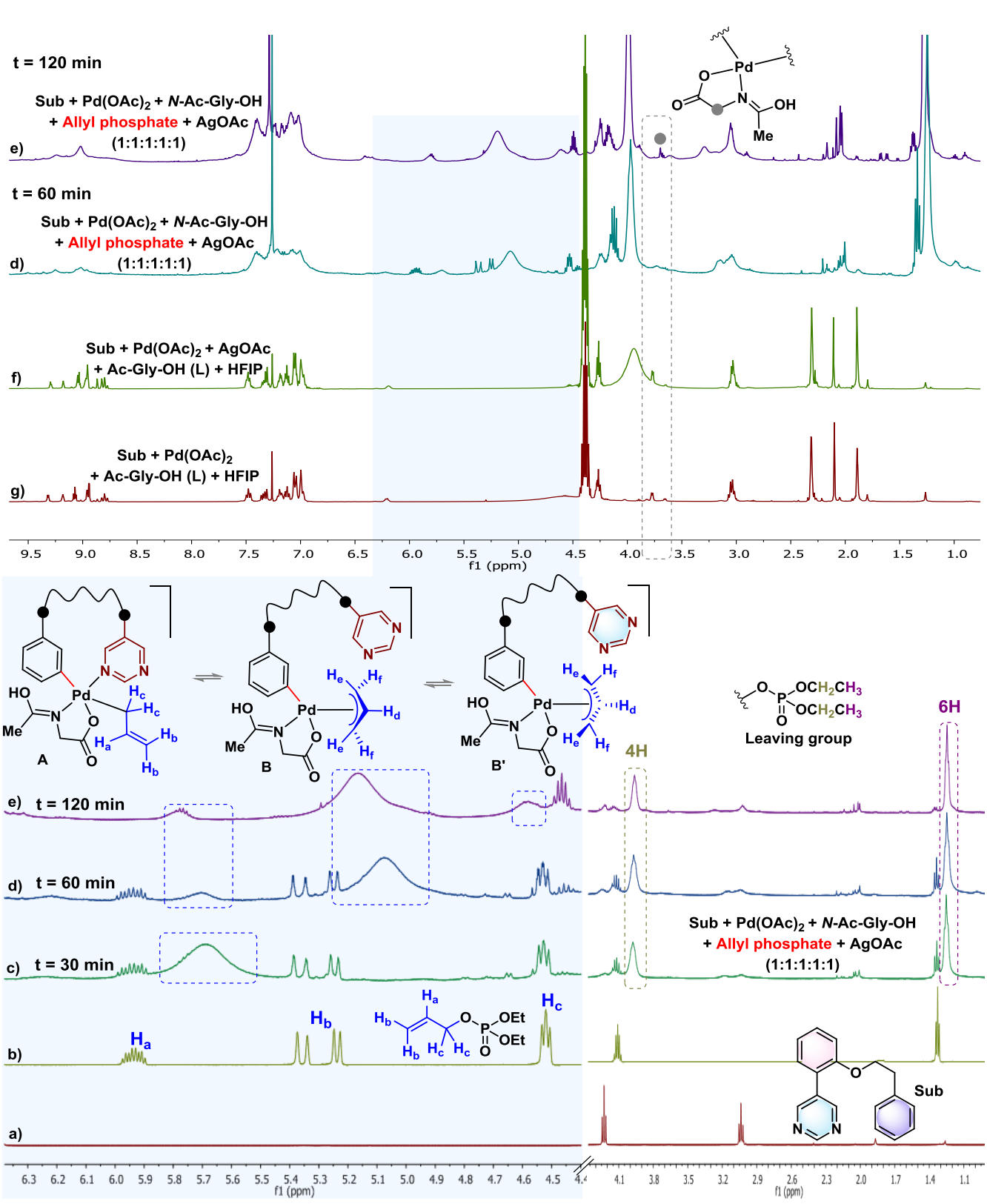

Figure 6. ^{1}H NMR of reaction mixture recorded at various time intervals to detect the η^3-Pd-π-allyl intermediate and phosphate release. Hydrogen-bonding and ionic charge are omitted due to clarity.[13]

mentioned protons where N and O atoms are interacting with HFIP. The chemical shifts of protons H_a, H_b, H_c, H_d and H_e of the substrate are indeed shifted upon addition of HFIP. This polar solvent is likely to have another role as well such as stabilization of cationic intermediates, or solubilizing the base, salt and the intermediates. ESI-MS studies of the reaction mixture,

in the absence of the allylating reagent, indeed indicated the formation of a macrocyclic palladacycle as shown in Figure 5.[13] Identification of such an intermediate can be considered as an evidence for a ligand assisted C–H activation in this example.

Subsequently, we focused on the allylation step more closely. The conventional allylation mechanism is mainly based on either metal insertion into olefin and subsequent elimination of the leaving group or through η^1-η^3 isomerized intermediate, followed by reductive elimination.[20,21] To determine the intermediate in the *meta*-allylation reaction with allyl phosphate, we have performed ^{1}H NMR studies of the crude reaction mixture (Figure 6). NMR results indicate an initial coordination of allyl phosphate with ligand-palladium complex and followed by oxidative addition of palladium into allyl phosphate to form an η^1-intermediate then rapid formation of η^3-intermediate (Figure 6, bottom spectra). Broadening of the spectra is likely an indication of a rapid η^1-to-η^3 isomerization *via* a σ-π interaction in Pd-π-allyl complex (in Figure 6; A, B and B').[21] To confirm the source of such broadening, we have compared the reaction mixture spectra in the presence of allyl phosphate with; 1) palladium acetate and *N*-Ac-Gly-OH and 2) palladium acetate, *N*-Ac-Gly-OH and silver acetate (Figure 6, top spectra). During rapid η^1-to-η^3 isomerization, the mixture contains chemically different protons in allyl moieties of **A**, **B** and **B'** (Figure 6). Due to rapid η^1-to-η^3 isomerization, the switching in chemical shift of all protons led to the broadening of spectra in the assigned region.[21] Investigation to detect π-allyl intermediate commenced by assigning of the peaks which revealed that no protons of the substrate and ligand *N*-Ac-Gly-OH are present in the mentioned region (Figure 6f and 6g).

Although the outgoing phosphate is visible in the spectra, it is rather difficult to ascertain whether the phosphate is bound to the palladium or remains as a counter anion. ^{31}P NMR of the crude reaction mixtures reveals the interaction of phosphate with palladium and silver (Figure 7).[13,22]

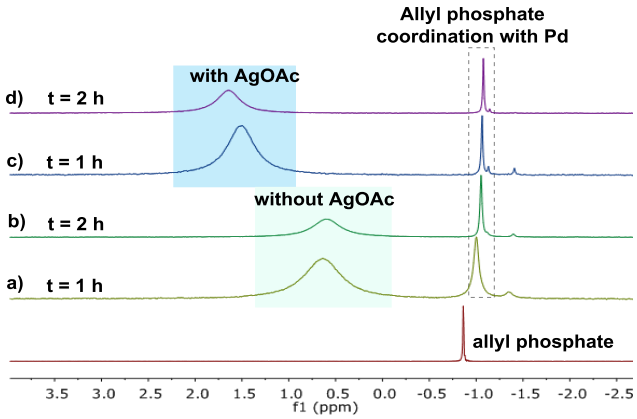

Figure 7. ^{31}P NMR of reaction mixture with and without of silver(I) acetate.

The formation of silver phosphate precipitate under the experimental condition most likely arises through these mechanistic steps. The next step is an allyl C–C bond formation between the Pd-bound allyl and aryl groups that results in the final product **P1**.

Role of different components on *meta*-allylation and kinetic studies. To gain more insights into catalytic cycle, we have carried out several spectroscopic and kinetic experiments. The initial rate of the reactions was determined by excluding different reagents such as catalyst, ligand, silver salt or additive from the standard condition. Desired allylation product was not detected in the absence of palladium-catalyst. Expectedly, sluggish reactivity was observed in the absence of *N*-Ac-Gly-OH (blue-colored curve) as well as silver(I) acetate (greenish blue-colored curve) whereas additive sodium triflate (red-colored curve) did not show much impact on initial reaction rate and the overall yield (Figure 8). Subsequently, kinetic studies were performed to determine the order with respect to substrate, allyl phosphate and palladium(II) acetate (Figures 9 and 10).

From the initial slope calculations, a first order rate dependency with respect to allyl phosphate and palladium acetate, and fractional order with respect to substrate were obtained.[13] Observed fractional order with respect to the substrate is likely due to the formation of a palladium-substrate complex, which is in pre-equilibrium with catalytically active palladium-substrate that delivers the product and another undesired palladium-substrate complex.[20b,23] The computational studies are consistent with carbon-carbon bond formation (*i.e.*, **P1**) from (η^1-allyl)palladium intermediate **6A** as the overall rate determining step

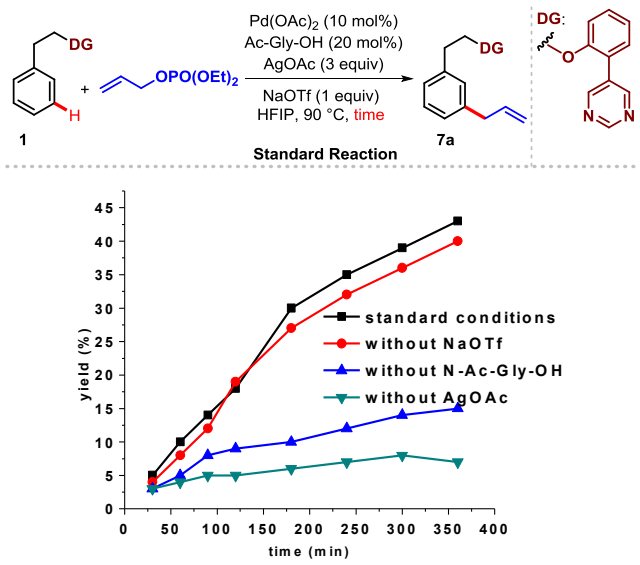

Figure 8. Control experiments by varying different reagents.

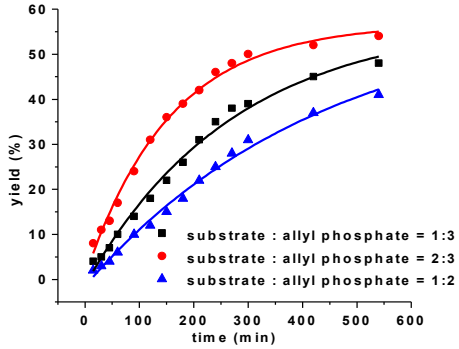

Figure 9. Order determination with respect to substrate and allyl phosphate.

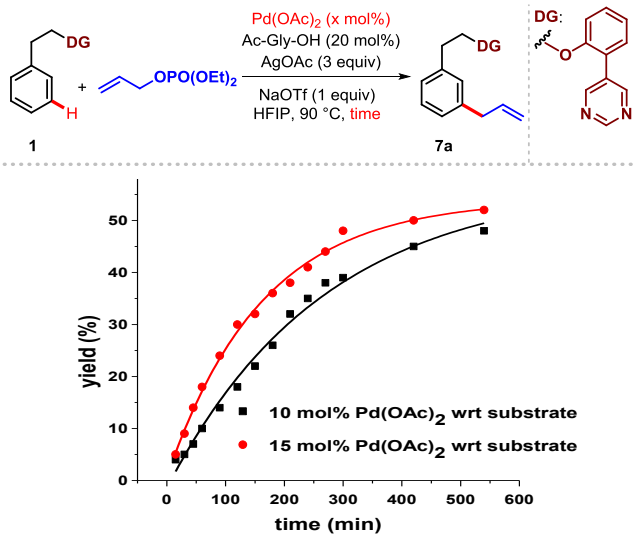

Figure 10. Order determination with respect to $Pd(OAc)_2$.

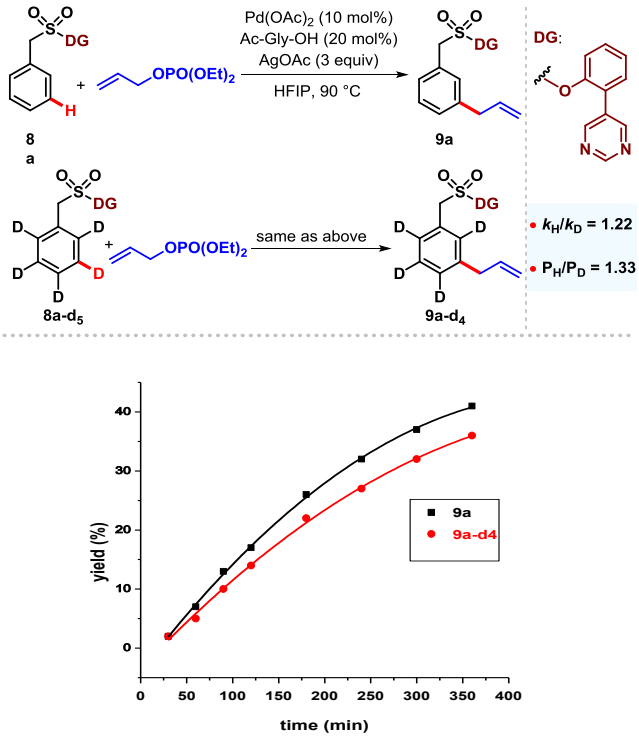

Figure 11. Kinetic isotope effect studies[13]

(RDS). The found order rate dependency on substrate and allyl phosphate indicates the C–H activation step is unlikely the rate-limiting step in overall reaction which was further confirmed by the intermolecular kinetic studies with protiated and deuterated-substrates (*i.e.*, k_H/k_D = 1.22 and P_H/P_D = 1.33) (Figure 11).[13,24]

Often in case of distal C–H functionalization, C–H activation is the rate determining step (RDS) as high energy is required to form the large macrocyclic transition state. However, the current kinetic isotope effect studies of allylation along with other functionalization with pyrimidine-based directing group such as *meta*-C–H cyanation[24b] revealed that k_H/k_D and P_H/P_D values are close to one and C–H activation step is no longer RDS. Even, the C–H activation step is no longer RDS in case of nitrile-based template mediated *meta*-C–H olefination by Yu group.[24c] Our recent report on *meta*-deuteration with pyrimidine-based scaffolds suggested that the C–H activation step can be reversible (see the Supporting Information).[15a]

Computational Studies. To probe the effectiveness of the pyrimidine-based directing group and the role of additives, we have carried out detailed density functional theory computations by using the B3LYP-D3 functional.[25] For easier comprehension, the following sections are organized into generation of potential active catalyst, discussion on the primary catalytic cycle without the silver salt, role of solvent HFIP as well as the silver salt.

First, we considered different ligand combinations around the Pd center and have identified an important species **A** that could serve as the potential active catalyst (Figure 12).[26] The active species **A** consists of Pd(II) center with a chelated N-acetyl glycinyl ligand, an acetic acid, and a HFIP as the other ligands. Similarly, we have considered hydrogen bonding interaction of solvent HFIP with the carbonyl oxygen of the N-acetyl glycinyl ligand in all the intermediates and transition states.[27]

The first step in the catalytic cycle **A** is the binding of substrate **1** to the Pd center through the pyrimidine-N by displacement of a molecule of acetic acid to form catalyst-substrate complex **1A** of energy -4.1 kcal/mol.[28] Expulsion of labile HFIP from the Pd center in **1A** can help in improving the proximity between the aryl group of the substrate the Pd as shown in intermediate **2A**. Herein we harness the experimental evidences, such as NMR detection of HFIP-bound intermediates such as **1A** and **2A** to narrow down the mechanistic possibilities that are considered for an in-depth computational study. The next step is a ligand-assisted *meta*-C–H bond activation *via* **TS1A** to form a palladacycle intermediate **3A**.[29] The ESI-MS studies of the reaction mixture, in the absence of the allylating reagent, indeed indicated the formation of a macrocyclic species as shown in Figure 5 (experimental part). Identification of **3A** could be considered as an evidence for a ligand assisted C–H activation in this example. An alternative possibility with explicit inclusion of silver salt was found to be of higher energy.[30] The next step in the catalytic cycle involves the binding of substrate allyl phosphonate (**R2**) to **3A** to form another intermediate **4A**. The mode of binding of **R2** is found to involve a key hydrogen-bonding between the enol proton of the *N*-acetyl glycinyl ligand and the phosphate oxygen. This mode of binding is energetically more preferred over an alternative direct coordination of the phosphate to the Pd center.[31] The transfer of allyl moiety to the Pd *via* **TS2A** can then provide an allyl-Pd(IV) intermediate (**5A**). Incoming of silver acetate and the decoordination of the pyrimidine DG in **5A** lead to the formation of **6A**. In **6A**, the acetate from the silver acetate was found to remain hydrogen bonded with the Pd-bound glycinyl ligand. The silver phosphate precipitate noted under the experimental condition most likely arises through these mechanistic steps. The next step is the C–C bond formation between the Pd-bound allyl moiety and the Pd-aryl group of the substrate via **TS3A** that leads to the final product **P1**.[32] As a result of this reductive elimination, Pd(IV) in **6A** goes the native Pd(II) oxidation state. The decoordination of the product **P1** from the catalyst can then regenerate the active species **A**.

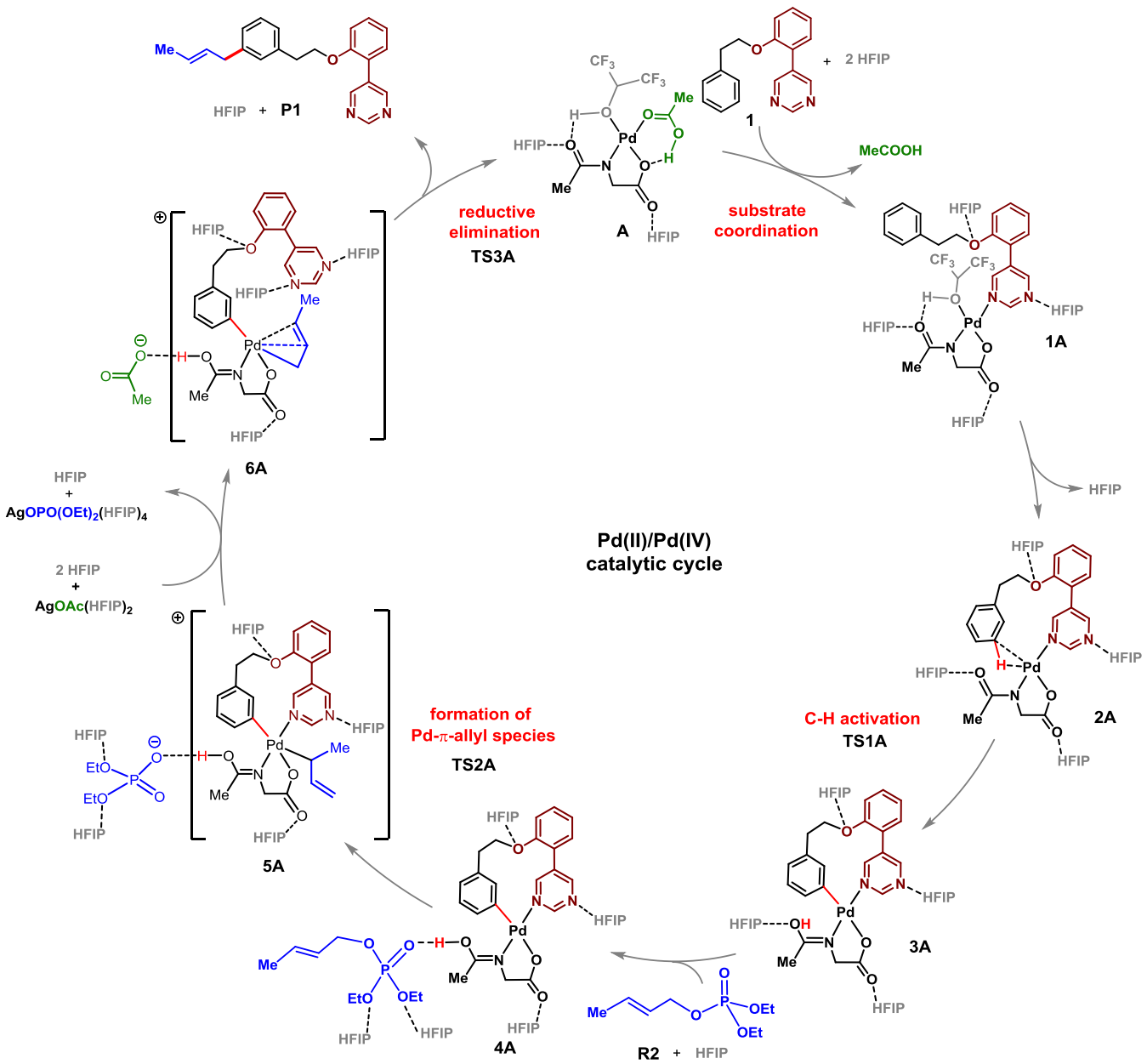

Figure 12. The mechanistic cycle for the Pd-catalyzed *meta*-allylation reaction without the explicit participation of silver salt.

The overall energetic features of this catalytic cycle can be understood by using the Gibbs free energy profile provided in Figure 13. It can be noticed that **TS3A** for the C–C bond formation with a relative Gibbs free energy of 27.0 kcal/mol is the highest energy point on the profile. The application of the *energetic span model* suggests that intermediate **1A** and **TS3A** are respectively the turn-over determining intermediate (TDI) and turn-over determining transition state (TDTS).[33] The energy difference of 31.1 kcal/mol between them is the energetic span (δE) for this catalytic cycle.

Next, we have examined the role of HFIP, first, by hypothesizing that the solvent HFIP might exert a critical role in the reaction mechanism since maximum yield was observed when HFIP is used as the solvent. Various possible *meta*-C–H activation transitions states, with and without explicit HFIP molecules bound to the substrate and/or catalyst, were considered to shed light on the role of HFIP (Figure 14). Among several possibilities, we note that **TS1A** with four HFIP molecules, two on the substrate and two on the Pd-*N*-acetyl glycinyl ligand, was energetically the most favorable one.[34] Interestingly, the NMR signatures as shown in Figure 4 (experimental part), are in line with the involvement of the HFIP-bound substrate. Hence, the ensuing intermediates and transition states with HFIP binding were considered in this study.

In addition, a greater number of noncovalent interactions between the HFIP molecule with both the substrate and the catalyst in the lower energy *meta*-C–H activation transition state **TS1A** compared to similar transition states **TS1A′** and **TS1A^0** with no or lesser number of explicit HFIP molecules.[35] These interactions help in lowering the energies of all such HFIP-bound stationary points. The lower yield for the reaction

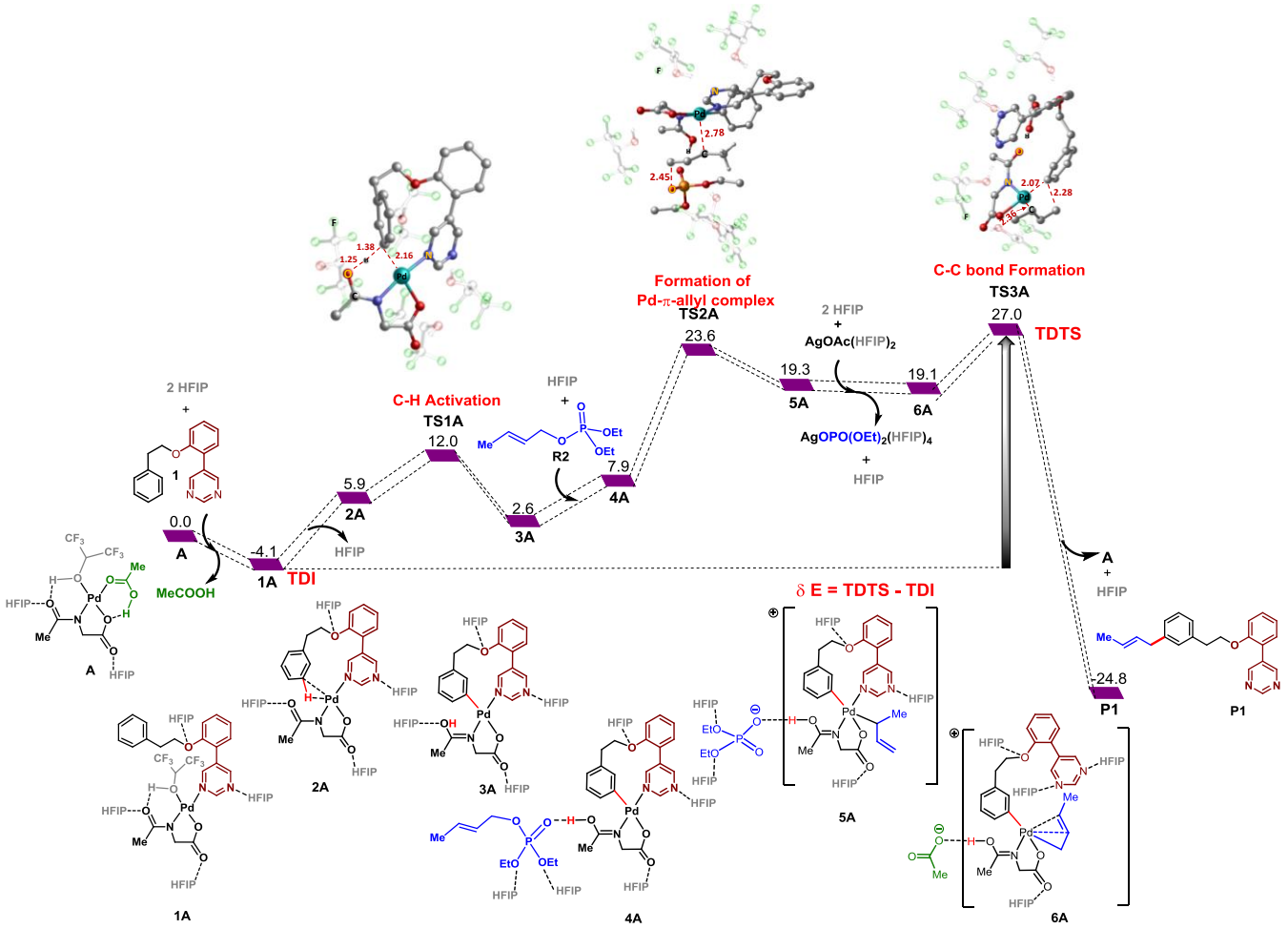

Figure 13. Gibbs free energy profile for *meta*-allylation reaction catalyzed by active species **A** as obtained at the SMD$_{(iso\text{-butanol})}$/B3LYP-D3/SDD(Pd),6-31G** level of theory. The relative Gibbs free energies (in kcal/mol) of intermediates and transition states are with respect to active species **A**.

observed with other solvents could be due to less effective interactions with such solvents other than HFIP. A comparison of the energies of all stationary points with and without explicit HFIP molecules indicates that the unique combination of template, solvent and allylating reagent are important to the present protocol. Thus, it can be concluded that the role of HFIP all through the catalytic cycle appears to be substantial.

Another important question pertaining to the regio- and chemoselectivities are addressed at this stage. Different modes of *ortho-*, *meta-*, and *para-* C–H activation transition states were

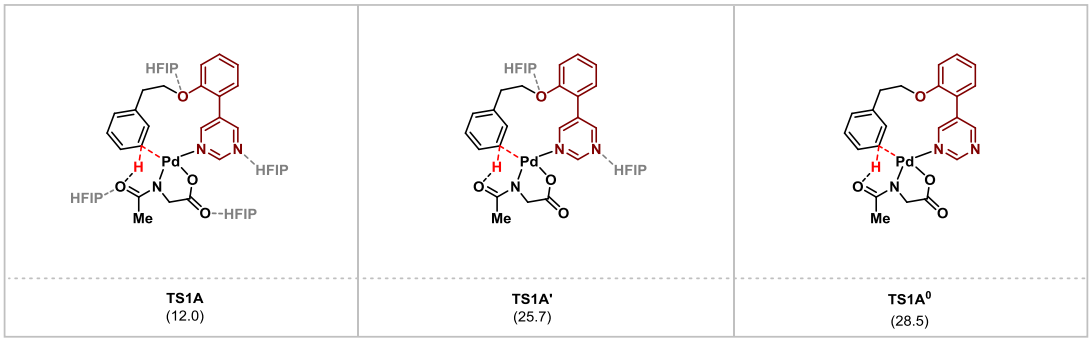

Figure 14. Qualitative representation of the *meta*-C–H activation transition states with and without bound HFIP molecules. The relative Gibbs free energies (in kcal/mol) of intermediates are respect to active species **A** and the separated reactants. The energies are obtained at the SMD$_{(iso\text{-butanol})}$/B3LYP-D3/SDD(Pd),6-31G** level of theory.

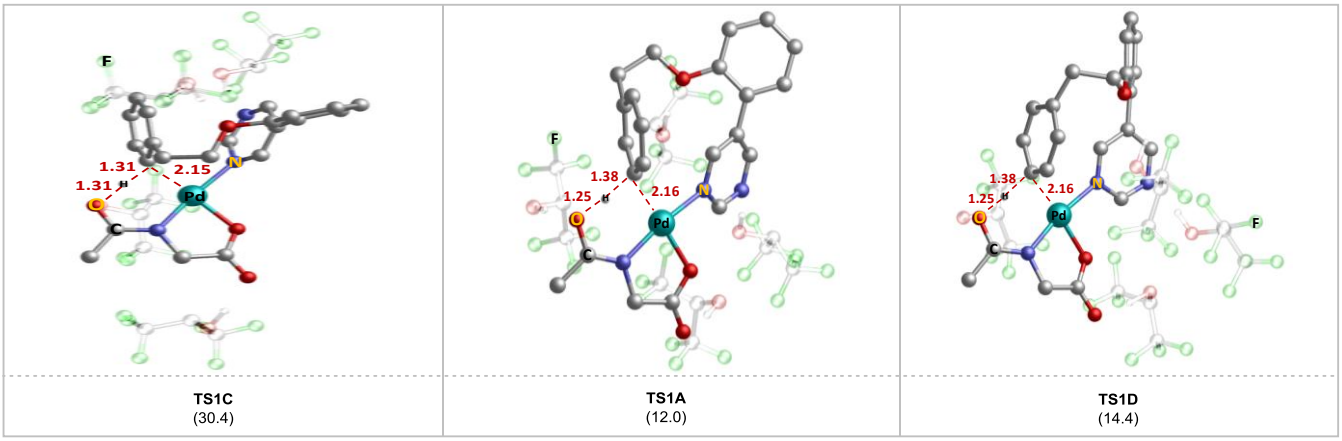

Figure 15. Optimized geometries and corresponding relative Gibbs free energies (in kcal/mol) for the ligand assisted *ortho*-, *meta*-, and *para*- C–H activation transition states, calculated with respect to the active species **A** and the separated reactants. The energies are obtained at the SMD$_{(iso\text{-butanol})}$/B3LYP-D3/SDD(Pd),6-31G** level of theory.

located in order to develop more understanding about why the present reaction offers *meta*.[36] The Gibbs free energies of ligand assisted transition states for the *ortho*- and *para*- C–H activation were found to be respectively 18.4 and 2.4 kcal/mol higher than that at the *meta*-position (Figure 15). The corresponding elementary step barriers with respect to the respective preceding intermediates for *ortho*-, *meta*-, and *para*- C–H activation transition states were found to be 23.4, 6.8 and 10.0 kcal/mol, respectively. These energetic details are line with the experimentally observed *meta* selective C–H activation. The reaction also yielded a branched minor product **P2**. This minor product is formed by the C–C bond formation between the more substituted allyl position and the aryl group via **TS4A** of energy 31.8 kcal/mol (Figure 16). The higher energy of **TS4A** compared to **TS3A** explains the formation of branched product as the minor product **P2**.

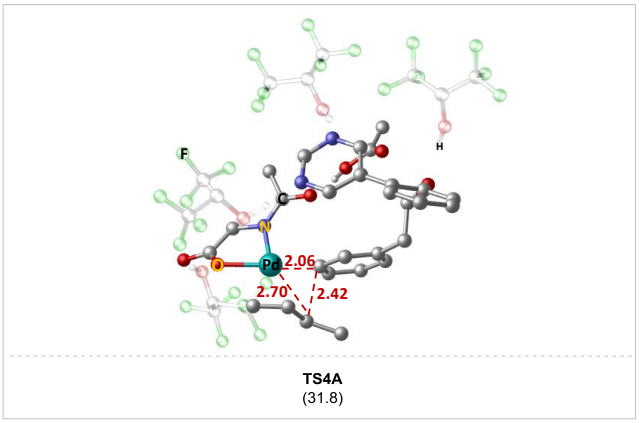

Figure 16. The optimized geometry of alternative transition state that lead to the branched product **P2** obtained at the SMD$_{(iso\text{-butanol})}$/B3LYP-D3/SDD(Pd),6-31G** level of theory.

The mechanistic studies showed that the solvent HFIP, pyrimidine directing group on the substrate and the *N*-acetyl glycinyl ligand play important roles. The pyrimidine directing helps in better coordination of the substrate to palladium center. Solvent HFIP lowers the energy of transition states and intermediates in the C–H activation step through hydrogen bonding interactions with the substrates as well as the *N*-acetyl glycinyl ligand of the catalyst. The silver salt additive has been found to play a key role in the allylation step by facilitating the removal of phosphate from the allyl phosphate. The turn-over determining transition state was found to be the C–C bond formation step that leads to the product.

CONCLUSION

We have explored the *meta*-C–H allylation with the aid of pyrimidine-based DG using various allyl phosphate as effective allylating reagent. The broad substrate scope has been presented with ether, sulfonyl and carbonyl ester linkages. Present protocol has been validated with long-chain ether-tethered substrates. Synthesis of eugenol derivative by applying the current protocol made this strategy attractive. The mechanistic studies showed that the solvent HFIP, pyrimidine directing group on the substrate and the amino acid ligand play important role. The pyrimidine directing group helps in better coordination of substrate to palladium center. While HFIP lower the energy of transition states and intermediates through its interactions with catalysts and substrates, MPAA ligand *N*-Ac-Gly-OH helps in C–H activation. The turn-over determining transition state were found to be the allyl C–C bond formation step that leads to the product.

ASSOCIATED CONTENT

Supporting Information. The supporting information includes experimental procedures, characterization data, and copies of NMR spectra for all products; computed energy components, Cartesian coordinates of all of the DFT-optimized structures is available free of charge on the ACS publications website at http://pubs.acs.org.

AUTHOR INFORMATION

Corresponding Author

*E-mail: dmaiti@chem.iitb.ac.in
*E-mail: sunoj@chem.iitb.ac.in

Notes

The authors declare no competing financial interest.

ACKNOWLEDGMENT

This activity was supported by SERB, India (CRG/2018/003915). Financial support from UGC (S.B. and S. K.) is gratefully acknowledged.

REFERENCES

(1) (a) Trost, B. M.; Toste, F. D. Enantioselective Total Synthesis of (−)-Galanthamine. *J. Am. Chem. Soc.* **2000**, *122*, 11262−11263. (b) Trost, B. M.; Thiel, O. R.; Tsui, H.-C. DYKAT of Baylis−Hillman Adducts: Concise Total Synthesis of Furaquinocin E. *J. Am. Chem. Soc.* **2002**, *124*, 11616−11617. (c) Webber, P.; Krische, M. J. Concise Stereocontrolled Formal Synthesis of (±)-Quinine and Total Synthesis of (±)-7-Hydroxyquinine *via* Merged Morita-Baylis-Hillman-Tsuji-Trost Cyclization. *J. Org. Chem.* **2008**, *73*, 9379−9387. (d) Bower, J. F.; Kim, I. S.; Patman, R. L.; Krische, M. J. Catalytic Carbonyl Addition through Transfer Hydrogenation: A Departure from Preformed Organometallic Reagents. *Angew. Chem. Int. Ed.* **2008**, *48*, 34−46. (e) Ni, G.; Zhang, Q.-J.; Zheng, Z.-F.; Chen, R.-Y.; Yu, D.-Q. 2-Arylbenzofuran Derivatives from Morus cathayana. *J. Nat. Prod.* **2009**, *72*, 966−968. (f) Alam, R.; Diner, C.; Jonker, S.; Szabó, K. J. Catalytic Asymmetric Allylboration of Indoles and Dihydroisoquinolines with Allylboronic Acids: Stereodivergent Synthesis up to Three Contiguous Stereocenters. *Angew. Chem. Int. Ed.* **2016**, *55*, 14417−14421. (g) Ketcham, J. M.; Volchkov, I.; Chen, T.-Y.; Blumberg, P. M.; Kedei, N.; Lewin, N. E.; Krische, M. J. Evaluation of Chromane-Based Bryostatin Analogues Prepared *via* Hydrogen-Mediated C–C Bond Formation: Potency Does Not Confer Bryostatin-Like Biology. *J. Am. Chem. Soc.* **2016**, *138*, 13415−13423. (h) Bailey, A. M.; Wolfrum, S.; Carreira, E. M. Biological Investigations of (+)-Danicalipin A Enabled Through Synthesis. *Angew. Chem. Int. Ed.* **2016**, *55*, 639−643.

(2) (a) Martín Castro, A. M. Claisen Rearrangement over the Past Nine Decades. *Chem. Rev.* **2004**, *104*, 2939−3002. (b) Maryasin, B.; Kaldre, D.; Galaverna, R.; Klose, I.; Ruider, S.; Drescher, M.; Kählig, H.; González, L.; Eberlin, M. N.; Jurberg, I. D.; Maulide, N. Unusual Mechanisms in Claisen Rearrangements: An Ionic Fragmentation Leading to a *meta*-Selective Rearrangement. *Chem. Sci.* **2018**, *9*, 4124−4131. (c) Lutz, R. P. Catalysis of the Cope and Claisen Rearrangements. *Chem. Rev.* **1984**, *84*, 205−247.

(3) Cope, A. C.; Hardy, E. M. The Introduction of Substituted Vinyl Groups. V. A Rearrangement Involving the Migration of an Allyl Group in a Three-Carbon System1. *J. Am. Chem. Soc.* **1940**, *62*, 441−444.

(4) (a) Rueping, M.; Nachtsheim, B. J. A Review of New Developments in the Friedel–Crafts Alkylation: From Green Chemistry to Asymmetric Catalysis. *Beilstein J. Org. Chem.* **2010**, *6*, 6. (b) Tao, Y.; Wang, B.; Zhao, J.; Song, Y.; Qu, L.; Qu, J. Friedel–Crafts-Type Allylation of Nitrogen-Containing Aromatic Compounds with Allylic Alcohols Catalyzed by a [$Mo_3S_4Pd(\eta^3$-allyl)] Cluster. *J. Org. Chem.* **2012**, *77*, 2942−2946.

(5) (a) Tsuji, J. Carbon-Carbon Bond Formation *via* Palladium Complexes. *Acc.Chem. Res.* **1969**, *2*, 144−152. (b) Trost, B. M.; Van Vranken, D. L. Asymmetric Transition Metal-Catalyzed Allylic Alkylations. *Chem. Rev.* **1996**, *96*, 395−422.

(6) (a) Zhang, Y. J.; Skucas, E.; Krische, M. J. Direct Prenylation of Aromatic and α,β-Unsaturated Carboxamides *via* Iridium-Catalyzed C−H Oxidative Addition−Allene Insertion. *Org. Lett.* **2009**, *11*, 4248−4250. (b) Asako, S.; Ilies, L.; Nakamura, E. Iron-Catalyzed *Ortho*-Allylation of Aromatic Carboxamides with Allyl Ethers. *J. Am. Chem. Soc.* **2013**, *135*, 17755−17757. (c) Ye, B.; Cramer, N. A Tunable Class of Chiral Cp Ligands for Enantioselective Rhodium(III)-Catalyzed C–H Allylations of Benzamides. *J. Am. Chem. Soc.* **2013**, *135*, 636-639. (d) Wang, H.; Schröder, N.; Glorius, F. Mild Rhodium(III)-Catalyzed Direct C–H Allylation of Arenes with Allyl Carbonates. *Angew. Chem. Int. Ed.* **2013**, *52*, 5386−5389. (e) Mishra, N. K.; Sharma, S.; Park, J.; Han, S.; Kim, I. S. Recent Advances in Catalytic C(sp^2)–H Allylation Reactions. *ACS Catal.* **2017**, 7, 2821–2847.

(7) (a) Chen, Z.; Wang, B.; Zhang, J.; Yu, W.; Liu, Z.; Zhang, Y. Transition Metal-Catalyzed C–H Bond Functionalizations by the Use of Diverse Directing Groups. *Org. Chem. Front.* **2015**, *2*, 1107−1295. (b) Rouquet, G.; Chatani, N. Catalytic Functionalization of C(sp2)-H and C(sp3)-H Bonds by Using Bidentate Directing Groups. *Angew. Chem. Int. Ed.* **2013**, *52*, 11726−11743.

(8) (a) Hofmann, N.; Ackermann, L. *Meta*-Selective C–H Bond Alkylation with Secondary Alkyl Halides. *J. Am. Chem. Soc.* **2013**, *135*, 5877−5884. (b) Tobisu, M.; Chatani, N. Remote Control by Steric Effects. *Science* **2014**, *343*, 850. (c) Kuninobu, Y.; Ida, H.; Nishi, M.; Kanai, M. A *meta*-Selective C–H Borylation Directed by a Secondary Interaction Between Ligand and Substrate. *Nat. Chem.* **2015**, *7*, 712. (d) Wang, X.-C.; Gong, W.; Fang, L.-Z.; Zhu, R.-Y.; Li, S.; Engle, K. M.; Yu, J.-Q. Ligand-Enabled *meta*-C–H Activation Using a Transient Mediator. *Nature* **2015**, *519*, 334. (e) Gemoets, H. P. L.; Laudadio, G.; Verstraete, K.; Hessel, V.; Noël, T. A Modular Flow Design for the *meta*-Selective C−H Arylation of Anilines. *Angew. Chem. Int. Ed.* **2017**, *56*, 7161−7165.

(9) (a) Leow, D.; Li, G.; Mei, T.-S.; Yu, J.-Q. Activation of Remote *meta*-C–H Bonds Assisted by an End-on Template. *Nature* **2012**, *486*, 518. (b) Yang, Y. F.; Cheng, G. J.; Liu, P.; Leow, D.; Sun, T. Y.; Chen, P.; Zhang, X.; Yu, J. Q.; Wu, Y. D.; Houk, K. N. Palladium-Catalyzed meta-Selective C−H Bond Activation with a Nitrile-containing Template: Computational Study on Mechanism and Origins of Selectivity. *J. Am. Chem. Soc.* **2014**, *136*, 344−355. (c) Cheng, G. J.; Yang, Y. F.; Liu, P.; Chen, P.; Sun, T. Y.; Li, G.; Zhang, X.; Houk, K. N.; Yu, J. Q.; Wu, Y. D. Role of N-Acyl Amino Acid Ligands in Pd(II)-Catalyzed Remote C−H Activation of Tethered Arenes. *J. Am. Chem. Soc.* **2014**, *136*, 894−897. (d) Bera, M.; Maji, A.; Sahoo, S. K.; Maiti, D. Palladium(II)-Catalyzed *meta*-C–H Olefination: Constructing Multisubstituted Arenes through Homo-Diolefination and Sequential Hetero-Diolefination. *Angew. Chem. Int. Ed.* **2015**, *54*, 8515−8519. (e) Li, S.; Ji, H.; Cai, L.; Li, G. Pd(II)-Catalyzed Remote Regiodivergent *ortho*- and *meta*-C–H Functionalizations of Phenylethylamines. *Chem. Sci.* **2015**, *6*, 5595−5600. (f) Dey, A.; Sinha, S. K.; Achar, T. K.; Maiti, D. Game of Directors: Accessing Remote *Meta*- and *Para*-C–H Bonds With Covalently Attached Directing Groups. *Angew. Chem. Int. Ed.* **2019**, *58*, 10820–10843.

(10) Bag, S.; Patra, T.; Modak, A.; Deb, A.; Maity, S.; Dutta, U.; Dey, A.; Kancherla, R.; Maji, A.; Hazra, A.; Bera, M.; Maiti, D. Remote *para*-C–H Functionalization of Arenes by a D-Shaped Biphenyl Template-Based Assembly. *J. Am. Chem. Soc.* **2015**, *137*, 11888−11891.

(11) *Meta*-selectivity is one of the major issues in the distal C–H functionalization. If there is regio-switchable coupling partner (linear *vs.* branched), it adds further selectivity issues. DG can lead to the *meta*- (major), *ortho*- and *para*- products formation. On the other hand, allyl coupling partner can provide linear as well as branched product and, in some cases, allyl can isomerize to olefin [Oi, S.; Tanaka, Y.; Inoue, Y. *Ortho*-Selective Allylation of 2-Pyridylarenes with Allyl Acetates Catalyzed by Ruthenium Complexes. *Organometallics* **2006,** *25*, 4773−4778]. Additionally, all regioisomers of allyl coupling partner can be present individually at *meta*-, *ortho*- and *para*- positions. Therefore, it is indeed a great challenge to achieve one product exclusively.

(12) Use of terminal olefin produces mixture of compounds including branched olefination, linear olefination, allylatation; whereas internal aliphatic olefin leads to tertiary carbon containing allylation product: Achar, T. K.; Zhang, X.; Mondal, R.; Shanavas, M. S.; Maiti, S.; Maity, S.; Pal, N.; Paton, R. S.; Maiti, D. Palladium-Catalyzed Directed *meta*-Selective C−H Allylation of Arenes: Unactivated Internal Olefins as Allyl Surrogates. *Angew. Chem. Int. Ed.* **2019**, *58*, 10353–10360.

(13) See the Supporting Information for detailed descriptions.

(14) Chu, L.; Shang, M.; Tanaka, K.; Chen, Q.; Pissarnitski, N.; Streckfuss, E.; Yu, J.-Q. Remote *Meta*-C–H Activation Using a Pyridine-Based Template: Achieving Site-Selectivity *via* the Recognition of Distance and Geometry. *ACS Cent. Sci.* **2015**, *1*, 394−399.

(15) (a) Bag, S.; Petzold, M.; Sur, A.; Bhowmick, S.; Werz, D. B.; Maiti, D. Palladium-Catalyzed Selective *meta*-C−H Deuteration of Arenes: Reaction Design and Applications. *Chem. Eur. J.* **2019**, *25*, 9433–9437. (b) Porey, S.; Zhang, X.; Bhowmick, S.; Singh, V.; Guin, S.; Paton, R. S.; Maiti, D. Alkyne Linchpin Strategy for Drug:Pharmacophore Conjugation: Experimental and Computational Realization of a *Meta*-Selective Inverse Sonogashira Coupling. *J. Am. Chem. Soc.* **2020**, *142*, 3762−3774.

(16) (a) Zhang, L.; Zhao, C.; Liu, Y.; Xu, J.; Xu, X.; Jin, Z. Activation of Remote meta-C–H Bonds in Arenes with Tethered Alcohols: A Salicylonitrile Template. *Angew. Chem. Int. Ed*. **2017**, *56*, 12245–12249. (b) Jayarajan, R.; Das, J.; Bag, S.; Chowdhury, R.; Maiti, D. Diverse meta-C-H Functionalization of Arenes across Different Linker Lengths. *Angew. Chem. Int. Ed*. **2018**, *57*, 7659 –7663.

(17) (a) Colomer, I.; Chamberlain, A. E. R.; Haughey, M. B.; Donohoe, T. J. Hexafluoroisopropanol as a highly versatile solvent. *Nat. Rev. Chem.* **2017**, *1*, 0088. (b) Sinha, S. K.; Bhattacharya, T.; Maiti, D. Role of hexafluoroisopropanol in C–H activation. *React. Chem. Eng*. **2019**, *4*, 244–253.

(18) (a) Wang, Y.; Gevorgyan, V. Synthesis of Active Hexafluoroiso-propyl Benzoates through a Hydrogen-Bond-Enabled Palladium(II)-Catalyzed C−H Alkoxycarbonylation Reaction. *Angew. Chem. Int. Ed*. **2017**, *56*, 3191−3195. (b) Parasram, M.; Gevorgyan, V. Silicon-Tethered Strategies for C−H Functionalization Reactions. *Acc. Chem. Res*. **2017**, *50*, 2038−2053.

(19) Lapointe, D.; Fagnou, K. Overview of the Mechanistic Work on the Concerted Metallation-Deprotonation Pathway. *Chem. Lett*. **2010**, *39*, 1118−1126.

(20) (a) Yao, T.; Hirano, K.; Satoh, T.; Miura, M. Stereospecific Copper-Catalyzed C−H Allylation of Electron-Deficient Arenes with Allyl Phosphates. *Angew. Chem. Int. Ed.* **2011**, *50*, 2990−2994. (b) Larsson, J. M.; Szabó, K. J. Mechanistic Investigation of the Palladium-Catalyzed Synthesis of Allylic Silanes and Boronates from Allylic Alcohols. *J. Am. Chem. Soc.* **2013**, *135*, 443−455. (c) Wang, Y.-M.; Buchwald, S. L. Enantioselective CuH-Catalyzed Hydroallylation of Vinylarenes. *J. Am. Chem. Soc.* **2016**, *138*, 5024−5027. (d) Guo, C.; Fleige, M.; Janssen-Müller, D.; Daniliuc, C. G.; Glorius, F. Cooperative N-Heterocyclic Carbene/Palladium-Catalyzed Enantioselective Umpolung Annulations. *J. Am. Chem. Soc.* **2016**, *138*, 7840−7843. (e) Rössler, S. L.; Krautwald, S.; Carreira, E. M. Study of Intermediates in Iridium–(Phosphoramidite,Olefin)-Catalyzed Enantioselective Allylic Substitution. *J. Am. Chem. Soc.* **2017**, *139*, 3603−3606. (f) Kim, S. W.; Zhang, W.; Krische, M. J. Catalytic Enantioselective Carbonyl Allylation and Propargylation *via* Alcohol-Mediated Hydrogen Transfer: Merging the Chemistry of Grignard and Sabatier. *Acc.Chem. Res.* **2017**, *50*, 2371−2380. (g) Sempere, Y. and Carreira, E. M. Trimethyl Orthoacetate and Ethylene Glycol Mono-Vinyl Ether as Enolate Surrogates in Enantioselective Iridium-Catalyzed Allylation. *Angew. Chem. Int. Ed.* **2018**, *57*, 7654−7658.

(21) (a) Solin, N.; Szabó, K. J. Mechanism of the η^3–η^1–η^3 Isomerization in Allylpalladium Complexes: Solvent Coordination, Ligand, and Substituent Effects. *Organometallics* **2001**, *20*, 5464-5471. (b) Pregosin, P. S. Phosphorus–olefin chelation in coordinated atropisomeric chiral auxiliaries. *Chem. Commun*. **2008**, 4875–4884.

(22) Chen, W.; Hartwig, J. F. Control of Diastereoselectivity for Iridium-Catalyzed Allylation of a Prochiral Nucleophile with a Phosphate Counterion. *J. Am. Chem. Soc.* **2013**, *135*, 2068−2071.

(23) (a) Das, A. K. Kinetic and mechanistic aspects of metal ion catalysis in cerium(IV) oxidation. *Coordination Chemistry Reviews* **2001**, *213*, 307–325. (b) Knipe, A. C. Organic Reaction Mechanisms 2007: An Annual Survey Covering the Literature Dated January to December 2007. *Volume 138 of Organic Reaction Mechanisms Series*. John Wiley & Sons, 2011. (c) Maity, S.; Kancherla, R.; Dhawa, U.; Hoque, E.; Pimparkar, S.; Maiti, D. Switch to Allylic Selectivity in Cobalt-Catalyzed Dehydrogenative Heck Reactions with Unbiased Aliphatic Olefins. *ACS Catal.* **2016**, *6*, 5493−5499. (d) Baccalini, A.; Vergura, S.; Dolui, P.; Maiti, S.; Dutta, S.; Maity, S.; Khan, F. F.; Lahiri, G. K.; Zanoni, G.; Maiti, D. Cobalt-Catalyzed C(sp2)−H Allylation of Biphenyl Amines with Unbiased Terminal Olefins. *Org. Lett.* **2019**, *21*, 8842−8846.

(24) (a) Simmons, E. M.; Hartwig, J. F. On the Interpretation of Deuterium Kinetic Isotope Effects in C–H Bond Functionalizations by Transition-Metal Complexes. *Angew. Chem. Int. Ed.* **2012**, *51*, 3066-3072. (b) Bag, S.; Jayarajan, R.; Dutta, U.; Chowdhury, R.; Mondal, R.; Maiti, D. Remote *meta*-C–H Cyanation of Arenes Enabled by a Pyrimidine-Based Auxiliary. *Angew. Chem. Int. Ed.* **2017**, *56*, 12538−12542. (c) Fang, L.; Saint-Denis, T. G.; Taylor, B. L. H.; Ahlquist, S.; Hong, K.; Liu, S.; Han, L.; Houk, K. N.; Yu, J.-Q. Experimental and Computational Development of a Conformationally Flexible Template for the *meta*-C−H Functionalization of Benzoic Acids. *J. Am. Chem. Soc*. **2017**, *139*, 10702−10714.

(25) (a) Lee, C.; Yang, W.; Parr, R. G. Development of the Colle-Salvetti Correlation-Energy Formula into a Functional of the Electron Density. *Phys. Rev. R.* **1998**, *37*, 785. (b) Grimme, S.; Antony, J.; Ehrlich, S.; Krieg, H. A Consistent and Accurate *ab initio* Parametrization of Density Functional Dispersion Correction (DFT-D) for the 94 Elements H-Pu. *J. Chem. Phys.* **2010**, *132*, 154104.

(26) See Figures S1, S2, S3 and Scheme S1 in the Supporting Information for additional details on different possible species considered as active species during the study.

(27) See Figure S4 in the Supporting Information for energy of different stationary points we considered without hydrogen bonding interaction with HFIP.

(28) See Figure S2 in the Supporting Information for additional details on different substrate binding possibilities considered during the study.

(29) See Figure S6 in the Supporting Information for details about different other *meta*-C–H activation transition states considered during the study.

(30) An alternative catalytic cycle **B** with explicitly included silver salt with species **B** as the active catalyst in Scheme S2 and Figure S5; and other possibilities are discussed in Figures S1 and S6 in the Supporting Information.

(31) See Figure S10 in the Supporting Information for details about coordination of R2 to Pd through O to form intermediate **4Aa**.

(32) See Figure S11 in the Supporting Information for details on alternative possibilities for reductive elimination transition states.

(33) (a) Kozuch, S.; Lee, S. E.; Shaik, S. Theoretical Analysis of the Catalytic Cycle of a Nickel Cross-Coupling Process: Application of the Energetic Span Model. *Organometallics* **2009**, *28*, 1303−1308. (b) Kozuch, S. A refinement of everyday thinking: the energetic span model for kinetic assessment of catalytic cycles. *Wiley Interdiscip. Rev. Comput. Mol. Sci.* **2012**, *2*, 795−815.

(34) (a) Bickelhaupt, F. M. Understanding reactivity with Kohn–Sham molecular orbital theory: E2–S_N2 mechanistic spectrum and other concepts. *J. Comput. Chem*. **1999**, *20*, 114. (b) Zeist W.-J. van; Bickelhaupt, F. M. The activation strain model of chemical reactivity. *Org. Biomol. Chem*. **2010**, *8*, 3118. (c) Ferna´ndez I.; Bickelhaupt, F. M. The activation strain model and molecular orbital theory: understanding and designing chemical reactions. *Chem. Soc. Rev*. **2014**, *43*, 4953. (d) Wolters L.P.; Bickelhaupt, F. M. The activation strain model and molecular orbital theory. *WIREs Comput. Mol. Sci.* **2015**, *5*, 324. (e) Bickelhaupt, F. M.; Houk, K. N. Analyzing Reaction Rates with the Distortion/Interaction-Activation Strain Model. *Angew. Chem. Int. Ed*. **2017**, *56*, 2. (e) See Figure S13 and Table S13 in the Supporting Information for details on how the *meta*-C–H activation transition states with and no HFIP are partitioned into fragments in *Activation Strain* analysis.

(35) (a) *AIM2000 Version 2.0*; Buro fur Innovative Software, SBK-Software, Bielefeld, Germany, 2002. (b) Bader, R. F. W. A quantum theory of molecular structure and its applications. *Chem. Rev*. **1991**, *91*, 893. (c) Biegler-Konig, F.; Schonbohm, J.; Bayles, D. AIM2000—A Program to Analyze and Visualize Atoms in Molecules. *J. Comput. Chem.* **2001**, *22*, 545. (d) See Figure S12 and Table S12 for Topological analysis of electron density using atoms in molecule analysis.

(36) See Figures S6, S7, S8, and S9 in the Supporting Information for additional details on different possible *ortho*-, *meta*- and *para*- C–H activation transition states considered during the study.

Table of Contents